J Solid State Electrochem (1997) 1: 126–133

ORIGINAL PAPER

J.L. Gautier · E. Meza · E. Silva · C. Lamas · C. Silva

Effect of the $ZnNi_yMn_{2-y}O_4$ ($0 \leq y \leq 1$) spinel composition on electrochemical lithium insertion

Received: 4 February 1997 / Accepted: 11 April 1997

Abstract The electrochemical insertion of lithium in the spinel-type manganite with the formula $ZnNi_yMn_{2-y}O_4$ has been studied. The galvanostatic discharge curves show that the best performance is obtained for $y = 0.25$, where a tetragonal to cubic structural transformation occurs. The thermodynamics and kinetics of the process of insertion of the lithium into the tetragonal spinel $Li_xZnNi_{0.25}Mn_{1.75}O_4$ ($x = 0.05$–1.3) have been studied. The molar thermodynamic quantities, such as enthalpy, entropy and free energy determined by EMF-T measurements, varied with the lithium concentration in the oxide structure, and a major variation was observed around $x = 0.8$. The chemical diffusion coefficient of lithium in these spinels was also determined. Structural analysis, degree of oxidation and magnetic susceptibility measurements were carried out for the lithiated oxides in order to obtain the cationic distribution as a function of x. It has been possible to demonstrate that, upon lithium insertion, Mn^{4+} ions on B sites are reduced to Mn^{3+} and then to Mn^{2+}. A cooperative Jahn-Teller effect is present in these spinel manganese-nickel oxides.

Key words Lithium insertion · Spinels · Mixed oxides · Zinc-nickel-manganese oxide · Lithium ion cells

J.L. Gautier (✉) · E. Meza
Laboratorio de Electroquímica,
Departamento de Química de Materiales,
Facultad de Química y Biología, Universidad de Santiago de Chile,
Casilla 33040, Santiago, Chile

E. Silva · C. Lamas · C. Silva
Departamento de Materiales Nucleares,
Comisión Chilena de Energía Nuclear,
Casilla 188-D, Santiago 1, Chile

Introduction

The electrochemical and chemical intercalation or insertion of lithium into transition metal oxides and chalcogenides exhibiting layered or tunneled structures has received considerable interest [1–4]. The main incentive has been the optimization of insertion electrodes in lithium ion ("rocking-chair") rechargeable batteries according to the main requisites: inexpensive, nontoxic, low equivalent weight and high energy density electrode compounds whose beneficial properties are due to the Li^+-ion mobility in the host material. Studies of topotactic lithium insertion/extraction, oxidation/reduction reactions in spinel oxides, mainly Fe_3O_4, Mn_3O_4, Co_3O_4, LiM_2O_4 (M = Ti, Mn, V) [5–10], and other more complex compounds such as $LiFe_5O_8$, $Li_2FeMn_3O_8$, $Li_2Mn_4O_9$, $Li_4Mn_5O_{12}$ [9–13] have demonstrated that they can accommodate at least one lithium ion per formula unit with fast Li^+ ion diffusion.

The spinel system is of particular interest because the Li^+ ions can be placed in the interstitial space defined by the $[B_2]O_4$ framework. It has been established that, during lithiation of spinel oxide compounds at room temperature, the $[B_2]O_4$ framework remains intact [14] while the A cations are displaced to an extra set of octahedral sites (16c). In a cubic spinel AB_2X_4 (Fd3m space group), the oxygen ions are the cubic close-packed anions X (32e position), the A and B cations are located in tetrahedral (8a) and octahedral (16d) sites, respectively, and the octahedral 16c sites are empty. The 64 tetrahedral interstices are at the three nonequivalent positions 8a, 8b and 48f. The interstitial space permitting 3D diffusion of lithium is composed of a three-dimensional network of tetrahedral (8a and 48f) and octahedral (16c) holes with shared faces. Cation distributions of $A[B_2]O_4$, $B[AB]O_4$ and $A_xB_y[A_{1-x}B_{1-y}]O_4$ give spinels classified as normal, inverse and mixed, respectively. It has been suggested for an iron spinel that the inserted lithium content decreases in the order inverse > mixed > normal spinels [9].

The electrochemical insertion process that corresponds to the discharge reaction of the Li cell involves the dissolution of x equivalents of Li ion from the intercalated anode (generally carbon compounds), their migration across the electrolyte and their insertion in the crystal structure of the semiconducting cathode compounds. The compensating electron travels in the external circuit to be finally injected into the electronic band. The reaction can be written as follows:

$$x\ \mathrm{Li}^{+}(\mathrm{host}) + (\mathrm{AB}_2)^{z+}_{\alpha}\mathrm{O}^{2-}_4 + x\ \mathrm{e}^{-} \rightarrow \mathrm{Li}^{+}_{x}(\mathrm{AB}_2)^{(z-\varepsilon)+}_{\alpha}\mathrm{O}^{2-}_4$$

α being the cationic nonstoichiometry and $\varepsilon = \mathrm{f}(x, \alpha)$.

Recently, manganese spinel compounds have attracted a considerable interest because of their attractive high-energy, low cost, nonpolluting features and their easy synthesis. Studies on the cathode materials $LiMn_2O_4$ [15–17], $Li_2Mn_2O_4$ [18], $Li_{1+x}Mn_2O_4$ [19], $Li_2Mn_4O_9$ and $Li_4Mn_5O_{12}$ [20] have been reported in recent years.

In this work we report lithium insertion reaction studies of the manganese spinel system $ZnNi_yMn_{2-y}O_4$ ($1 \geq y \geq 0$) aimed at understanding the role of ionic structure in this process. We have chosen the Zn-Ni-Mn-O system for the following reasons: (a) the existence of a structural transition tetragonal→cubic has been already detected [21], and (b) there is a practical interest in nickel oxides for battery applications [22].

Experimental

The individual polycrystalline spinels of the $ZnNi_yMn_{2-y}O_4$ ($1 \geq y \geq 0$) system were prepared at 400°C from aqueous solutions containing molar quantities of high-purity $Zn(NO_3)_2 \cdot 4\ H_2O$, $Ni(NO_3)_2 \cdot 6\ H_2O$ and $Mn(NO_3)_2 \cdot 4\ H_2O$ (Merck) slightly acidified with HNO_3 using the thermal decomposition method. The black mixture obtained was pelletized and calcined in a Pt crucible at 950°C. The pellet was then ground and again pelletized and calcined, ensuring decomposition to oxide. Total calcination time was 24 h. The fine powder (325 mesh) so obtained was kept under an inert atmosphere. Chemical analysis by atomic absorption (Perkin Elmer 403) confirmed the cationic stoichiometry. Thermogravimetric (Nerzsch STA-409) measurements were performed from room temperature up to 1450°C to check the oxygen stoichiometry. The typical heating rate was 5°C min^{-1}.

Formation of the spinel was confirmed by classical X-ray powder diffraction techniques (Siemens D5000) using CuK_α ($\lambda = 0.229092$ nm) radiation selected through a graphite monochromator.

Electrochemical measurements were carried out using two- and three-electrode cells. These were assembled in a dry box under a high-purity argon atmosphere and the cathode was separated from the lithium disc anode (99.9% Aldrich) by a porous glass paper disc soaked with the electrolyte (1 M $LiClO_4$ in PC or PC:EC).

The cathode pellet (5.5-mm thickness, 0.24-cm^2 surface) obtained at 500 psi was a mixture of the prepared oxide with acetylene black as a conducting agent and a teflon suspension (UCAR) as a binding agent, in a weight ratio of 90:5:5. Lithium ribbons were used as reference and counter electrodes.

The lithium insertion was achieved at 40 μA cm^{-2} (as determined in previous experiments) using a potentiostat/galvanostat device manufactured at the University of Santiago. The oxide electrode composition was changed by coulometric titration and the analysis of the experimental data was accomplished with a 486 microcomputer. Equilibrium was considered to be reached when the potential did not change by more than 0.001 V during 24 h. For further details, see [20]. To obtain cyclic voltammetry curves, an EG & G 273A potentiostat at a 1 mV s^{-1} scan rate between 0 and 3.5 V vs Li was employed. The chemical diffusion coefficient of Li^+ ions in the spinel samples was measured using the current pulse relaxation (CPR) technique [23], maintaining a constant current density of 0.42 mA cm^{-2} for 20 s.

The magnetic susceptibility (288–330 K) was recorded by the Faraday method, using a Cahn magnetobalance RTL 700 corrected for diamagnetic contributions.

Spectroscopic FTIR analyses were performed using a Bruker Fourier Transform spectrophotometer IFS 66V to evaluate the strength of MO_6 and MO_4 sublattice bonds. The degree of oxidation of the samples as a function of the degree of lithiation was determined by chemical reduction of the M^{n+} cations with $n \geq 2$ to $n = 2$ by vanadyl sulfate solutions [24].

Results and discussion

Control of oxides $ZnNi_yMn_{2-y}O_4$ ($1 \geq y \geq 0$)

The $ZnNi_yMn_{2-y}O_4$ (y = 0, 0.25, 0.5, 0.75 and 1) oxides synthesized by the described technique were analyzed by X-ray diffraction. The diffraction peaks of the oxides were indexed by comparison with the diffraction pattern of $ZnMn_2O_4$ and $NiMn_2O_4$ and were found to be in good agreement with the ASTM X-ray powder data files ICPDS-ICDD 1–1110 ($ZnMn_2O_4$) and 24–1133 ($NiMn_2O_4$), thus showing that the samples crystallized in a simple spinel phase without impurities. The brown color of the $ZnMn_2O_4$ spinel gradually turned black upon manganese substitution by nickel. A tetragonal phase is obtained for $y = 0$ and $y = 0.25$, whereas for all other compositions the oxides exhibit cubic spinel structure. Table 1 shows the a and c unit cell parameters obtained using a structure-refining computer program [25], the maximum error being 10^{-4} Å. The degree of tetragonality (measured by the c/a' ratio) decreases with the degree of manganese substitution by nickel, probably because of a cooperative Jahn-Teller effect. This effect is known to be due to Mn^{+3} (d^4) ions placed on B sites of the spinel [26]. The increase of Ni^{2+} concentration on B sites is in agreement with the observed structure change. In fact, according to the literature, two limits are possible: $Zn^{2+}[Mn^{3+}_2]O_4 (y = 0)$ and $Zn^{2+}[Ni^{2+}Mn^{4+}]O_4 (y = 1)$ [27].

The oxides turn out to be very stable compounds as no measurable weight loss was observed in the TGA

Table 1 Cell parameters of the oxides $ZnNi_yMn_{2-y}O_4$

y	a (Å)	c (Å)	a' (Å)	c/a'
0	5.716	9.253	8.456	1.094
0.25	5.720	9.196	8.443	1.089
0.5	8.345	8.345	–	1
0.75	8.337	8.337	–	1
1	8.333	8.333	–	1

analysis up to 1200°C where finally a loss of oxygen occurs. The oxygen stoichiometry of all compounds was verified.

The degree of oxidation is closely related to the increase in the Mn^{4+} concentration on the octahedral sites of the spinel oxide as has been shown in [21].

Electrochemical insertion

Lithium insertion in the oxides $ZnNi_yMn_{2-y}O_4$ with nickel stoichiometries $y = 0$, 0.25, 0.5, 0.75 and 1 was studied at room temperature using a cell of the type

$(-)$Li / electrolyte/$ZnNi_yMn_{2-y}O_4(+)$

Although experiments with spinels as cathodes were usually performed with 1 $MLiClO_4$-propylene carbonate (PC) (e.g. [9]), a second electrolyte containing a 1:1 mixture of PC and ethylene carbonate (EC) was also used [28]. This solution was checked in this work by sweep voltammetry measurements.

Before starting the experiments, the open circuit voltage (OCV) of the cell, which is a function of nickel, was set between 3.2 ($y = 0$) and 3.3 V ($y = 1$). Typical discharge curves at $j = 40$ μA cm^{-2} are reported in Fig. 1. After an initial part characterized by several slope changes, it is quite evident that the line shape and the extension of the plateau are a function of the degree of manganese substitution by nickel. It is easy to demonstrate for $y = 0$ and $y = 1$ that the degree of insertion is very low in the case of the nickel compositions, particularly in the range of the structural change. This is a very important point. The electrode is stable during the discharge curve. No cracks and no breaking into pieces was observed during dismantling of the cell.

It follows from Fig. 2 that the maximum degree of insertion of lithium requires a critical concentration of Mn^{4+} ions in the $[B_2]O_4$ sublattice of those Zn-Ni-Mn-containing spinels which result from a replacement of Mn^{+3} by Ni^{+2} ions. Some authors have established that this distortion takes place when 60% of the distorting

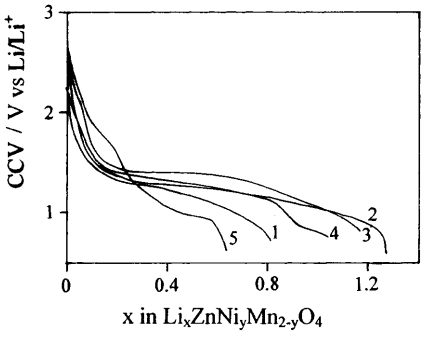

Fig. 1 Lithium insertion curves at $j = 40$ μA cm^{-2} for $ZnNi_yMn_{2-y}O_4$ oxides as a function of y (*1*) y = 0, (*2*) 0.25, (*3*) 0.5, (*4*) 0.75, (*5*) 1

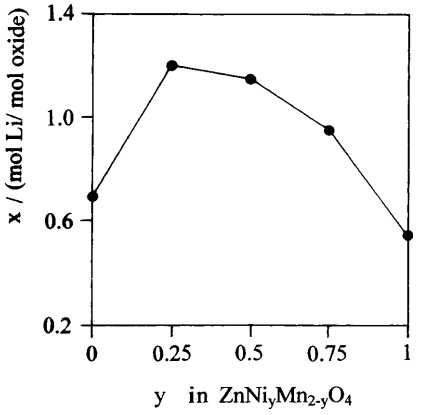

Fig. 2 Degree of lithium insertion vs nickel stoichiometry in $Li_xZnNi_yMn_{2-y}O_4$

Table 2 Tetragonal and cubic spinel cell parameters as a function of degree of lithium insertion into $Li_xZnNi_{0.25}Mn_{1.75}O_4$. a' cubic equivalent spinal cell parameter $= (2 \cdot a^2 \cdot c)^{1/3}$

x Mol lithium/mol oxide	a (Å)	c (Å)	a' (Å)	c/a'
0	5.720	9.196	8.443	1.089
0.05	5.720	9.203	8.445	1.090
0.1	5.721	9.237	8.456	1.092
0.5	5.724	9.249	8.462	1.093
1	5.729	9.240	8.465	1.092
1.2	5.723	9.259	8.465	1.094

Mn^{3+} ions are replaced in B_2O_4 [29]. It is not possible to admit the migration of manganese ions to tetrahedral sites displacing the Zn^{2+} ions from the AO_4 sublattice because these ions possess a high stabilization energy [30]. The Li ion insertion in the oxide $ZnNi_{0.25}Mn_{1.75}O_4$ increases the a' cell parameter (as cubic spinel) (Table 2). It can be seen that all lithiated oxide forms a tetragonal spinel phase.

Cyclic voltammetry

The reactivity of the cathode was checked by cyclic voltammetry. It can be seen that a nonmeasurable current is observed using carbon black-PTFE/$LiClO_4$ (EC:PC 1:1)/Pt (Fig. 3, curves 4 and 5). Using carbon black, the voltage range which may be explored without decomposing the electrolyte can be expanded into the cathodic region. In fact, electrolyte decomposition can occur when the cell oxide-PTFE/$LiClO_4$ (PC)/Li is used (Fig. 3, curve 1). The use of the mixture PC:EC 1:1 (curve 2) shifts the process to negative potentials. Note that employing $LiClO_4$ in PC:EC instead of in PC only as electrolyte enlarges the inert potential window (1.1 V to 3 V range).

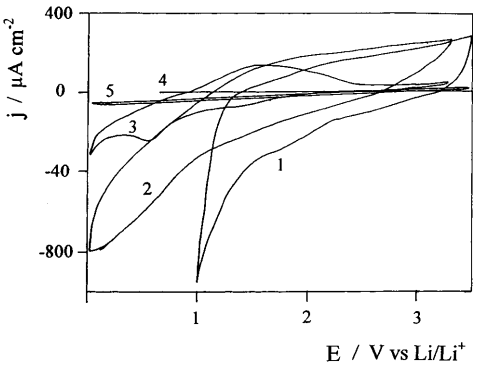

Fig. 3 Cyclic voltammograms of (*1*) Li/1 M $LiClO_4$ (PC)/$ZnNi_{0.25}Mn_{1.75}O_4$, (*2*) Li/0.5 M $LiClO_4$ (PC:EC 1:1)/$ZnNi_{0.25}Mn_{1.75}O_4$, (*3*) Li/0.5 M $LiClO_4$ (PC:EC 1:1)/$Li_{0.5}ZnNi_{0.25}Mn_{1.75}O_4$, (*4*) Li/0.5 M $LiClO_4$ (PC:EC 1:1)/C-Teflon bonded, (*5*) Pt/0.5 M $LiClO_4$ (PC:EC 1:1)/Pt

Determination of the chemical diffusion coefficients of Li^+ ions in $Li_xZnNi_yMn_{2-y}O_4$

The cyclic behavior of the lithiated oxide ($x = 0.5$) (Fig. 3, curve 3) has shown a low polarization between charge and discharge, suggesting that the kinetics of the lithium insertion process is not slow. To further explore this point, the chemical diffusion coefficients of Li^+ were determined. For each electrode material, the measurements were collected during the discharge curve using the CPR technique, for which the following equation was used:

$$E = IV_m\tau(dE/dx)/FA(\pi Dt)^{1/2} \quad (1)$$

I being the current pulse, V_m the molar volume, t the duration of the current pulse, dE/dx the local slope of the quasi-OCV vs x curve, and A the geometric electrode surface area.

The variation of the relaxation of the electrode potential as a function of $1/\sqrt{t}$ was perfectly linear. The D values, calculated from the slope of the lines, are represented in Fig. 4. It is important to note that the diffusion coefficient of Li^+ ions in the positive electrode material $Li_xZnNi_yMn_{2-y}O_4$ is independent of y for $0.75 > y > 0.25$ from $x = 0.4$ to $x = 0.8$, with a value in the order of 10^{-12} cm^2 s^{-1}. High D values at $x = 0.4$ for $y = 0$ and $y = 1$ were observed. In the case of a low degree of insertion ($x < 0.4$), the D values obtained are very high, 10^{-8} cm^2 s^{-1}, showing reasonable mobility of Li^+ ions for rocking-chair batteries. The temperature effect on D in the range 290–330 K is shown in Fig. 5. A linear relationship between log D and T^{-1} is obtained. The energy of activation of the diffusion process is low at a high concentration of inserted lithium and increases when x increases in the oxide. These phenomena can be related to the lattice spinel deformation as a function of x. In fact, the c/a' ratio changes with x from 1.089 ($x = 0$) to 1.094 ($x = 1.2$) (Table 2) facilitating the diffusion process through the spinel framework. FTIR analysis of the lithiated spinel as a function of x show four IR bands according to Waldron's theory [31]. We have used the main bands v_1 and v_2 that can be attributed to tetrahedral and octahedral frequencies, respectively [32]. It can be seen from Table 3 that no modification of the octahedral strength constant k_o is observed, whereas the tetrahedral strength constants k_t are significantly modified. A balance between the degree of insertion x and the value of the diffusion coefficient of Li^+ ions in the positive electrode material must be performed for their use as cathodes in batteries. From this point of view, the $ZnNi_{0.25}Mn_{1.75}O_4$ spinel oxide was studied.

Table 3 FTIR spectroscopic parameters and strength constants for the octahedral and tetrahedral M-O bond as a function of degree of lithium insertion

x	v_1 (cm^{-1})	v_2 (cm^{-1})	$k_T \times 10^5$ (mol/s^2)	$k_o \times 10^5$ (mol/s^2)
0	619.6	502.7	1.29	1.85
0.05	620.7	500.8	1.27	1.84
0.1	622.7	507.1	1.33	1.88
0.5	626.9	499.9	1.39	1.83
1	628.0	499.5	1.41	1.83
1.2	627.9	499.6	1.42	1.83

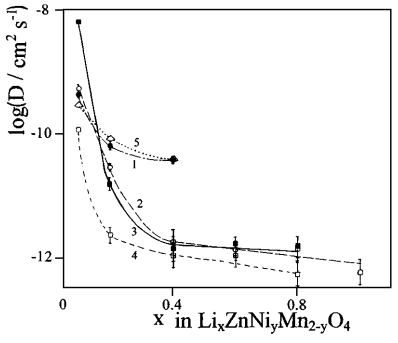

Fig. 4 Chemical diffusion coefficient of lithium in $ZnNi_yMn_{2-y}O_4$ as a function of nickel content at 298 K. (*1*) y = 0, (*2*) 0.25, (*3*) 0.5, (*4*) 0.75, (*5*) 1

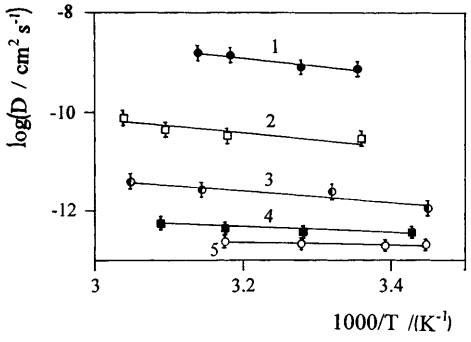

Fig. 5 Chemical diffusion coefficient of Li^+ vs temperature at different x. (*1*) $x = 0.05$, (*2*) 0.1, (*3*) 0.5, (*4*) 1.2, (*5*) 1.3

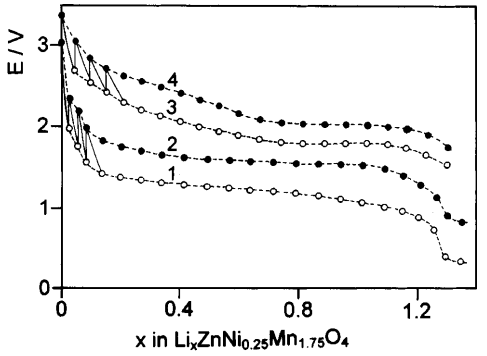

Fig. 6 Closed circuit (CCV) and open-circuit potentials (OCV) as a function of x in $Li_xZnNi_{0.25}Mn_{1.75}O_4$ at 25°C (*1*, *2*) and 55°C (*3*, *4*). (*1*, *3*) CCV, (*2*, *4*) OCV

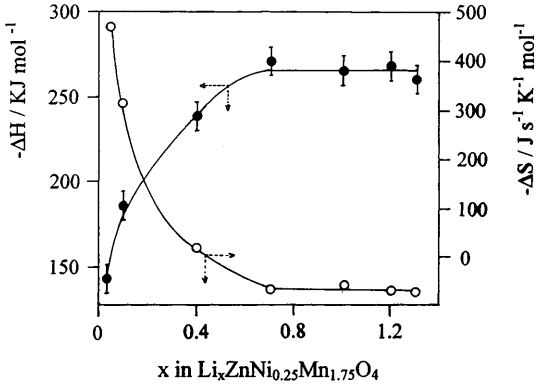

Fig. 8 Partial molar enthalpy and entropy as a function of x in $Li_xZnNi_{0.25}Mn_{1.75}O_4$

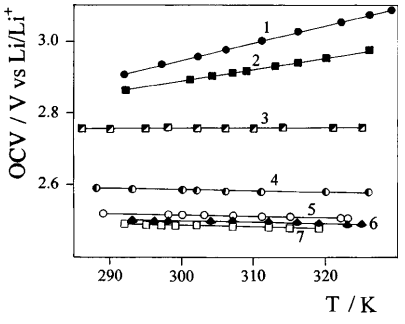

Fig. 7 Open-circuit voltage vs temperature as a function of x. (*1*) $x = 0.04$, (*2*) 0.1, (*3*) 0.4, (*4*) 0.7, (*5*) 1, (*6*) 1.2, (*7*) 1.3

Thermodynamics of the insertion of lithium into $Li_xZnNi_{0.25}Mn_{1.75}O_4$

Thermodynamic information on the lithium insertion process into $Li_xZnNi_{0.25}Mn_{1.75}O_4$ was obtained from EMF measurements on the basis of the following equations:

$$\Delta\overline{H}_{\mathrm{Li}(x,T)} = F[T(\partial E/\partial T)_x - E] \quad (2)$$

$$\Delta\overline{S}_{\mathrm{Li}(x,T)} = F(\partial E/\partial T)_x \quad (3)$$

$\Delta\overline{H}_{\mathrm{Li}(x,T)}$ and $\Delta\overline{S}_{\mathrm{Li}(x,T)}$ being the partial molar enthalpy and entropy of lithium insertion into the oxide host lattice, respectively, and E the EMF of the $Li/Li^+/Li_xZnNi_{0.25}Mn_{1.75}O_4$ cells.

The quasi-equilibrium open-circuit potential (OCV) or EMF curves E vs x for $Li_xZnNi_{0.25}Mn_{1.75}O_4$ electrodes are given in Fig. 6. It is interesting to note that constant potential plateaus are observed at both temperatures. EMF-temperature measurements were performed in the range from 288 to 325 K with good stability of the EMF. Typical EMF-T curves are shown in Fig. 7 for different x values of $Li_xZnNi_{0.25}Mn_{1.75}O_4$. Linear variations are observed through the x range, and in almost all cases the Li/oxide cells have a positive temperature coefficient dE/dT. The variation of the partial enthalpy for the lithium insertion corresponding to the reaction

$$ZnNi_{0.25}Mn_{1.75}O_4 + x\ Li^+ + x\ e \rightarrow Li_xZnNi_{0.25}Mn_{1.75}O_4 (1.3 > x > 0)$$

is shown in Fig. 8 as a function of the x value. It can be stated that the enthalpy $-\Delta\overline{H}_{\mathrm{Li}}$ increases with x up to $x \approx 0.7$ and then assumes a stable value. This may mainly be due to an increase in the interaction energy between the lithium and the oxide caused by a decreasing coulombic interaction energy between the inserted lithium ions. In fact, the contribution of the enthalpy $\Delta\overline{H}_{\mathrm{Li}}$ to the activity of the Li^+ ions inserted into the oxide framework is known to depend on (a) the energy arising from a strong interaction of lithium with the oxide structure, (b) repulsive interactions between inserted Li^+ ions, and finally (c) the energy required to modify the crystal framework sufficiently to accommodate the Li^+ ions inserted in the interstices. The values of the partial molar entropy of Li insertion, $\Delta\overline{S}_{\mathrm{Li}}$, obtained according to Eq. 3, are also shown in Fig. 8. For low lithium content ($x < 0.8$), high values of entropy are found, which may reflect a high degree of disorder. A further lithium insertion results in a decrease in $\Delta\overline{S}_{\mathrm{Li}}$, and, at around $x = 0.7$, reaches a minimum value. The high entropy values can be the consequence of a high mobility or a high vibrational freedom of lithium inserted in the oxide. It is obvious from the thermodynamic behavior of the oxide that lithium ordering takes place in the $Li_xZnNi_{0.25}Mn_{1.75}O_4$ spinel. The molar Gibbs free energy for the process can also be determined from $E(x,T)$ or EMF values. The $\Delta\overline{G}_{\mathrm{Li}}$ values must decrease with increasing lithium concentration in the oxide structure as the EMF values change because $\Delta\overline{G}_{\mathrm{Li}(x,T)} = -FE_{(x,T)}$. Gibbs free energies for the lithium insertion reaction at 298 K and 328 K were −101 and −271 kJ mol^{-1}, respectively. These results are similar to those reported for manganites, $Li_xMn_2O_4 \cdot y\ V_2O_5$ ($y = 0.25$ and 0.5) [23].

Table 4 Observed and calculated degree of oxidation for the oxides $Li_xZnNi_{0.25}Mn_{1.75}O_4$

x	$q(x)_{exp}$	$q(x)_{calc}$
0	2.01 ± 0.06	2
0.05	1.96 ± 0.06	1.95
0.1	1.85 ± 0.08	1.9
0.5	1.49 ± 0.03	1.5
1.0	1.04 ± 0.06	1
1.2	0.83 ± 0.01	0.8

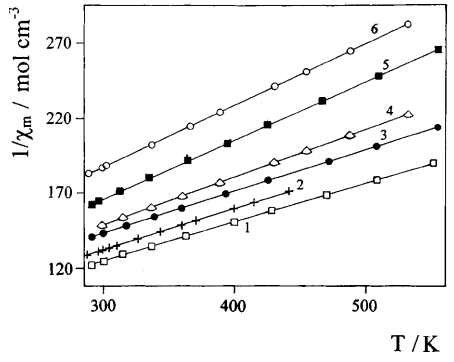

Fig. 9 Inverse susceptibility as a function of temperature for $Li_xZnNi_{0.25}Mn_{1.75}O_4$. (*1*) $x = 0$, (*2*) 0.05, (*3*) 0.1, (*4*) 0.5, (*5*) 1, (*6*) 1.2

Ionic distribution variation of $Li_xZnNi_{0.25}Mn_{1.75}O_4$ with lithium insertion

The host oxide $ZnNi_{0.25}Mn_{1.75}O_4$ can accommodate approximately one inserted lithium ion per formula unit. The unit cell volume of the $LiZnNi_{0.25}Mn_{1.75}O_4$ phase is only ~0.2% larger than that of the host phase. Upon lithium insertion, the axial ratio of the host compound is increased, as has already been shown (Table 2). The increase in the c parameter with x suggests that the Mn^{3+} ion concentration in the oxide lattice is increased as the charge-compensating electrons from inserted Li ions reduce the Mn^{4+} ions to Mn^{3+}, occupying the d states of the host lattice in octahedral sites. This conclusion is further supported by the decreasing degree of oxidation with x (Table 4) and an oxide distribution through the spinel cation sites.

The $Li_xZnNi_{0.25}Mn_{1.75}O_4$ phases must be normal spinels because Zn^{2+} ions probably occupy the 8a sites due to their strong preference for the tetrahedral sites [28], and all others ions are located in the octahedral framework. The interstitial Li ions could then only be placed in 16c sites.

The temperature variation of magnetic susceptibility of the lithiated oxide is shown in Fig. 9. A linear relationship is observed between χ_m^{-1} and T as is characteristic for the Curie-Weiss law $\chi = C(T-\theta)^{-1}$ in the explored temperature range (290–550 K). These lines, which are functions of x, have been used to obtain the effective magnetic moment of the oxide, $\mu_{eff} = \sqrt{8C}$ where C is the Curie constant. The theoretical values of μ_{eff} per formula weight were calculated by the equation

Table 5 Cationic distribution of oxides as a function of x

x	Ionic distribution
0	$Zn^{2+}[zn^{2+}_{0.25}Mn^{3+}_{1.5}Mn^{4+}_{0.25}]O^{2-}_4$
0.05	$(Li^{+}_{0.05})Zn^{2+}[Ni^{2+}_{0.25}Mn^{3+}_{1.55}Mn^{4+}_{0.2}]O^{2-}_4$
0.1	$(Li^{+}_{0.1})Zn^{2+}[Ni^{2+}_{0.25}Mn^{3+}_{1.6}Mn^{4+}_{0.15}]O^{2-}_4$
0.5	$(Li^{+}_{0.5})Zn^{2+}[Ni^{2+}_{0.25}Mn^{3+}_{1.5}Mn^{2+}_{0.25}]O^{2-}_4$
1	$(Li^{+})Zn^{2+}[Ni^{2+}_{0.25}Mn^{3+}Mn^{2+}_{0.75}]O^{2-}_4$
1.2	$(Li^{+}_{1.2})Zn^{2+}[Ni^{2+}_{0.25}Mn^{3}_{0.8}Mn^{2+}_{0.95}]O^{2-}_4$

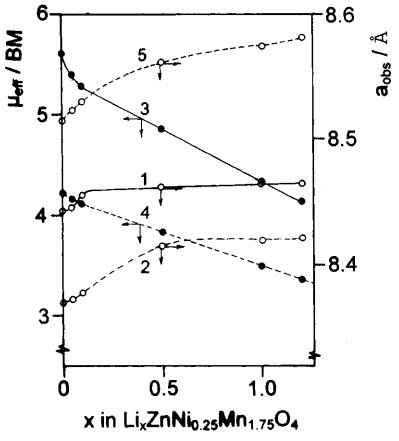

Fig. 10 Cell parameter and effective magnetic moment as a function of degree of lithium insertion degree (1) a-cell parameter observed, (2) a cell parameter calculated considering Mn^{II} and Mn^{III} in low spin state, (3) effective magnetic moment observed, (4) effective magnetic moment calculated considering Mn^{II} and Mn^{III} in low spin state, (5) cell parameter calculated considering Mn^{II} in low spin and Mn^{3+} in high spin state

$\mu_{eff} = (\Sigma c_i \mu_i)^{1/2}$ where μ_i is the classical magnetic moment of the ith ion in a given coordination and c_i its relative amount.

Correlations of various properties have been attempted in order to propose the ionic distribution of the cations at tetrahedral and octahedral sites in the spinel structure as a function of the degree of lithium insertion. For the deduction of a formula for each composition, the ionic partition of the host oxide $ZnNi_{0.25}Mn_{1.75}O_4$, which has been reported by us previously, has been used [21]. It has been proposed that for manganese-zinc spinels and manganese-nickel spinels prepared at high temperatures, as in this work, Mn^{3+}, Mn^{4+} and Ni^{2+} can exist at octahedral sites [27, 29]. To obtain the probable cationic distribution, we have used the relationship of Poix [33], which allows the cell parameters of oxides to be estimated on the basis of the cation-oxygen length of the ions placed at the different sites and the similarity between μ_{eff} calculated as a function of oxide composition to the observed μ_{eff}. Several distributions were tested. The results shown in Table 5 are in very good agreement with the experimental and calculated degrees of oxidation (Table 4). The calculated and observed structural parameters a

and μ_{eff} are given in Fig. 10. It can be observed that the trends are similar for both parameters a and μ_{eff}. However, an important difference between the experimental and the calculated results is obvious. The results are very sensitive to the ionic radius, the oxidation state and the spin state of the cations. The observed results (Fig. 10 curve 1 cell parameter, curve 3 magnetic moment) were matched more closely by calculated results considering Mn^{2+} and Mn^{3+} ions in the low-spin state (Fig. 10 curves 2 and 4). In fact, if Mn^{3+} is considered in the high-spin state, the a parameter is very high for all cases (Fig. 10 curve 5). Using Mn^{2+} and Mn^{3+} both in the high-spin state, or low- and high-spin state combinations, the results are very different from the experimental ones. In general, the cations were mostly assigned to the kind of position they are known to occupy in many mixed oxides. Taking the following reaction as the lithium insertion reaction in our oxides:

$$Zn^{2+}Ni^{2+}_{0.25}Mn^{z+}_{1.75}O_4 + x\ Li^+ \rightarrow Li^+_x Zn^{2+}Ni^{2+}_{0.25}Mn^{\delta+}_{1.75}O_4$$

where $\delta = z - x/1.75$, the theoretical z and δ values are in agreement with the values of degree of oxidation (Table 4). From the results shown in Table 5 it is clear that the interstitially inserted lithium in the $Li_xZnNi_{0.25}Mn_{1.75}O_4$ spinel reduces all surface Mn^{4+} ions first to Mn^{3+} ions and then to Mn^{2+} ions via electrochemical reduction. When $0.1 \geq x \geq 0$, the Mn^{4+} ions concentration decrease and Mn^{3+} increase at B sites in the same quantity as x. Therefore the pathway of the first lithium insertion will be:

$$\left(Zn^{2+}\right)_{8a}\left[Ni^{2+}_{0.25}Mn^{3+}_{1.5}Mn^{4+}_{0.25}\right]_{16d}O_4 \xrightarrow{x Li^+} \left(Zn^{2+}\right)_{8a}\left(Li^+_x\right)_{16c} \times \left[Ni^{2+}_{0.25}Mn^{3+}_{1.5+x}Mn^{4+}_{0.25-x}\right]_{16d}O_4$$

Conclusion

Electrochemical lithium insertion in the $ZnNi_yMn_{2-y}O_4$ spinel oxide was investigated. The discharge curves show a maximum reactivity (in terms of the amount of lithium ions inserted) for $ZnNi_{0.25}Mn_{1.75}O_4$, where a tetragonal $\rightarrow$ cubic structural change of the spinel occurs. The lithium insertion reaction was also studied using this nickel-zinc manganite as the electrode. Major variations in the thermodynamic and kinetic characteristics of Li insertion into the crystal lattice of $Li_xZnNi_{0.25}Mn_{1.75}O_4$ were observed at $x \approx 1$, which may be correlated with the oxide cationic distribution. The lithium ion can diffuse into the spinel structure at 16c vacant sites without modification of the bond strength between the octahedral cations and the oxygen.

We have tried to find a correlation between the cationic distribution in the oxide and the lithium insertion of these materials. The structure, composition, degree of oxidation and magnetic behavior have all been considered in order to derive the formula of the lithiated oxide. The results show that, in parallel with the lithium insertion into the nickel-zinc manganites, the reduction of the manganese B sites ($Mn^{4+} \rightarrow Mn^{3+} \rightarrow Mn^{2+}$) must occur, making the couple Mn^{4+}/Mn^{3+} of fundamental importance to the explanation of the observed reactivity of the oxide.

Since lithiation is an oxidation/reduction reaction in which ions and electrons are transferred from guest species to the host matrix, the facility of the host structure to receive extra electrons is essential when a cathode material is used in secondary lithium batteries. This can be accomplished by the right choice of the spinel framework.

Acknowledgements Financial assistance from CONICYT (project 1950542), DICYT-USACH and CCHEN is gratefully acknowledged. J.L.G. acknowledges English language suggestions by a referee.

References

1. Goodenough JB (1990) In: Akridge JR, Balkanski M (eds) Solid state microbatteries. Nato ASI series, Plenum, New York, vol 217, p 213
2. West K, Zachau-Chistiansen B, Jacobsen T, Skaarup S (1991) In: Nazri GA, Shriver DF, Huggins RA, Balkanski M (eds) Solid state ionics. Mat Res Soc Symp Proceedings Pittsburg vol 210, p 449
3. Scrosati B (1994) In: Lipkowski J, Ross PN (eds) Electrochemistry of novel materials. CCH, N.Y., p 111
4. Pistoia G (ed) (1995) Lithium batteries. Industrial Chem Library, vol 5
5. Thackeray MM, David WYF, Goodenough JB (1982) Mat Res Bull 17: 785
6. Thackeray MM, David WYF, Bruce PG, Goodenough JB Mat Res Bull 18: 461
7. Thackeray MM, Johnson PJ, Picciotto LA de, Bruce PG, Goodenough JB (1984) Mat Res Bull 19: 179
8. Thackeray MM, Baker SD, Adendorff KT, Goodenough JB (1985) Solid state ionics 17: 175
9. Chen CJ, Greenblatt M, Waszczak JV (1986) Mat Res Bull 21: 609
10. Picciotto LA de, Thackeray MM (1985) Mat Res Bull 20: 187
11. Rossouw MH, Kock A de, Picciotto LA, Thackeray MM, David WYF, Ibberson RM (1990) Mat Res Bull 25: 175
12. Kock A de, Rossouw MH, Picciotto LA de, Thackeray MM, David WYF, Ibberson RM (1990) Mat Res Bull 25: 657
13. Lubin F, Lecerf A, Broussely M, Labat Y (1991) J Power Sources 34: 161
14. Cava RJ, Murphy DW, Zahurak S (1984) J Solid State Chem 53: 64
15. Guyomard D, Tarascon JM (1992) J Electrochem Soc 139: 937
16. Yamada A, Miura K, Hinokuma K, Tanaka M (1995) J Electrochem Soc 142: 2149
17. Li W, Mc Kinnon WR, Dahn JR (1994) J Electrochem Soc 141: 2310
18. Tarascon JM, Guyomard D (1993) J Electrochem Soc 138: 2864
19. Guyomard D, Tarascon JM (1993) J Electrochem Soc 140: 3071
20. Gautier JL, Barbato S, Lamas C, Silva C (1994) Nucleotécnica 14: 29
21. Gautier JL, Bustos P, Trollund E, Brenet J (1983) Electrochim Acta 28: 1889

22. Delmas C, Saadune Y, Auradau H, Menetrier M, Hagenmuller P (1992) In: Chowdari BV (ed) Solid state ionics: materials and applications. World Sci, Singapore, p 255
23. Kumagai N, Fujiwara T, Tanno K (1993) J Electrochem Soc 140: 3197
24. Wickam DG, Whipple ER (1963) J Anal Chem 10: 314
25. Mueller MH, Heaton L, Miller KT (1960) Acta Cryst 13: 828
26. Goodenough JB (1973) Les oxydes des métaux de transition. Gauthier Villards, Paris
27. Ghare DG, Sinha APB (1968) J Phys Chem Solids 29: 885
28. Alcántara R, Morales J, Tirado JL, Stoyanova R, Zhecheva E (1995) J Electrochem Soc 142: 3997
29. Irani KS, Sinha EPB, Biswas AB (1960) J Phys Chem Solids 17: 101
30. Paul A, Basu S (1974) Trans J Br Ceramic Soc 73: 167
31. Waldron RD (1955) Phys Rev 99: 1727
32. Allen GC, Paul M (1995) Appl Spectrosc 49: 451
33. Poix P (1965) Bull Soc Chim Fr, 1085